Polymer 55 (2014) 1875–1882

Contents lists available at ScienceDirect

Polymer

journal homepage: www.elsevier.com/locate/polymer

Alignment and reordering of a block copolymer by solvent-enhanced thermal laser direct write

Jonathan P. Singer [a,b,1], Kevin W. Gotrik [a,2], Jae-Hwang Lee [c], Steven E. Kooi [b], Caroline A. Ross [a], Edwin L. Thomas [a,b,c,*]

[a] Department of Materials Science and Engineering, Massachusetts Institute of Technology, Cambridge, MA 02139, USA
[b] Institute for Soldier Nanotechnologies, Massachusetts Institute of Technology, Cambridge, MA 02139, USA
[c] Department of Mechanical Engineering and Materials Science, Rice University, Houston, TX 77005, USA

ARTICLE INFO

Article history:
Received 7 January 2014
Received in revised form
6 February 2014
Accepted 7 February 2014
Available online 15 February 2014

Keywords:
Block copolymer
Laser heating
Zone annealing

ABSTRACT

Block copolymer (BCP) thin films have shown high potential as a pattern transfer medium for ultra-fine (<20 nm) features. We introduce an effective approach for performing rapid local annealing of BCP films by focused laser spike (FLaSk) zone annealing, using a moving highly-focused circularly polarized visible wavelength laser spot. A poly(styrene-b-dimethylsiloxane) BCP was transformed from a metastable spherical micelle morphology to the bulk equilibrium cylindrical morphology aligned along the write direction within a region controlled by manipulation of the laser focal plane, even for curved paths. This simultaneous microdomain reordering and alignment was accomplished on the *tens of millisecond* time scale by creating a very large driving thermal gradient (estimated as 100–750 K/μm or, temporally, 3000 –75,000 K/s), enhanced by incorporation of solvent vapor (here toluene) swelling of the BCP film. The extent of the thermal effects suggests that the role of solvent may extend beyond increasing the mobility of the BCP film to enhancing both the thermal gradient and also potentially the surface energy gradients, providing a thermocapillary shear mechanism. Further, enhanced domain alignment is greatest at higher scan speed, indicating as well the importance of the *temporal* thermal gradient.

1. Introduction

Well-ordered thin films of microphase-separating block copolymer (BCP) domains are commonly assembled through the use of thermal annealing processes which allows the kinetically trapped, as-cast polymer microdomain structure to attain the equilibrium morphology *via* diffusion by increasing temperature to overcome the energetic barrier for chain reptation [1]. Several techniques for controlling the orientation, morphology, and long range order of the BCP microdomains have been developed, in particular, substrate patterning to direct the self-assembly by chemical epitaxy [2,3] and graphoepitaxy [4–9]. As an alternative or supplement to thermal annealing, solvent vapor annealing involves placing the BCP in a vapor environment where solvent molecules can diffuse into the film and plasticize the polymer, decreasing the glass transition temperature and improving the mobility of the BCPs for self-assembly at ambient temperatures [10]. Solvent annealing can produce non-equilibrium morphologies if the solvent is selective to one of the blocks, changing the effective volume fraction, as has recently been studied in detail for poly (styrene-*b*-dimethylsiloxane) (PS-PDMS) cylindrical BCP [11–13]. Techniques for the generation of BCP films containing regions of different microdomain types (*e.g.* coexisting regions of spheres and cylinders) have also been investigated. These methods involve trapping the BCP in a first morphology determined by one annealing process, then immobilizing the chains in regions of the film by crosslinking to fix one of the two microphases. Both e-beam [4,14] or ultraviolet [14] exposure can be used to fix the initial microdomain structure. Then a further annealing step with a different (or no) solvent can produce a second morphology in the un-crosslinked regions. The second solvent annealing step has been accomplished locally with a direct write solvent vapor nozzle without the need for crosslinking [15].

* Corresponding author. George R. Brown School of Engineering, MS-364, P.O. Box 1892, Houston, TX 77251, USA. Tel.: +1 713 348 4955; fax: +1 713 348 5300.
E-mail address: elt@rice.edu (E.L. Thomas).
[1] Current address: Yale University, Department of Chemical and Environmental Engineering, 9 Hillhouse Ave, Mason 222, New Haven, CT 06511, USA.
[2] Current address: 3M Corporate Research Process Lab, 3M Center, 0218-01-S-05, St. Paul, MN 55144, USA.

http://dx.doi.org/10.1016/j.polymer.2014.02.028
0032-3861/

Most recently, spatially controlled positioning, thickness and tuning within the microphase diagram was demonstrated by electrohydrodynamic jet printing of multiple compositions of a BCP, including graphoepitaxy and chemical epitaxy for enhanced ordering and alignment [16].

While these techniques enable feature control down to the length scale of a single microdomain (using e-beam cross-linking), most require the inclusion of crosslinkable block chemistry and possibly an additional crosslinking initiator and in the absence of templating, do not provide control over the in-plane microdomain orientation or registration that may be desirable for subsequent pattern transfer applications. In order to develop a more general technique that enables both localized morphology and orientational control with short annealing times, we investigated focused laser spike (FLaSk) zone annealing as a route to BCP patterning and sub-second annealing.

Laser spike annealing (LSA) has been utilized as an alternative to a standard thermal treatment in semiconductor technology [17–19] and also for the annealing of soft materials, such as chemically amplified photoresists [20,21] and for BCP microphase separation [22]. In this technique, a high intensity continuous or pulsed laser is rapidly scanned across an absorbing surface, such as a silicon wafer substrate supporting the device or polymer film. The local temperature at the laser spot spikes to a high value and then, once the laser light is removed, very rapidly drops back to ambient temperature. Because of this, both the temperature and annealing time of the thin film can be controlled by selection of laser intensity and exposure time. Additionally, annealing can be performed while avoiding unwanted effects, such as material degradation or diffusion. For BCP systems, the first demonstration of LSA was performed in 2007 and utilized a high power (on the order of a Watt), ms pulsed CO_2 laser exposure, which could initiate microphase separation for ~1 min total exposures, but did not demonstrate good domain ordering and often resulted in considerable polymer damage including burning and void formation, ostensibly due to intrinsic optical absorption and degradation of the polymer [22].

In considering LSA of a thin BCP film, there are obvious similarities to zone annealing, a technique previously utilized for both thin and thick films of BCP for achieving simultaneous annealing and alignment. In zone annealing, a BCP film is moved over an induced thermal gradient resulting in alignment along the direction of the motion over the heat source. One important distinction among various zone annealing techniques is whether they are 'hot' (above the order-disorder transition (ODT)) [23,24] or 'cold' (below ODT) [25–27] at their maximum temperature. In both cases, microdomain ordering and alignment happens primarily in the regions of the thermal gradient: for hot zone annealing, ordering occurs as the BCP passes back through its ODT, while in cold zone annealing it was shown that a majority of ordering occurs in the cold-to-hot portion of the gradient and was relatively independent of subsequent baking, indicating the importance of a gradient for driving the reordering and alignment of the domains [25]. A combined approach of cold zone annealing with thermal expansion-induced surface shear by a top PDMS film resulted in exceptionally high order and alignment for annealing rates of up to 200 μm/s (traveling through a 0.045 K/μm, 9 K/s gradient) and film thicknesses from a single layer of microdomains up to 1 μm [28]. Additionally, it was shown that without the presence of the top PDMS layer, thermal gradients of a similar magnitude could lead to vertical alignment with respect to the substrate [29], which was most recently used to accomplish roll-to-roll perpendicular alignment of BCP domains [30].

We introduced FLaSk annealing which utilizes continuous wave visible or near-IR light and a high numerical aperture objective (in this study, NA = 0.4) to accomplish LSA on a micron or sub-micron scale, for the post-exposure bake of absorbing-dye-doped chemically amplified resists [31] and, more recently, for thermocapillary dewetting of polymer thin films [32]. Here, as in the latter study, we utilize a FLaSk technique similar to conventional LSA in that it takes advantage of the quasi-2D absorption of the substrate to generate heat (Fig. 1), but still allows for LSA on a region of polymer of limited size, creating an effective instantaneous confinement by the surrounding unheated immobile polymer. As with conventional LSA, the duration, effective size, and temperature of this confined annealing are controllable by the laser power, writing speed, and tightness of focus. Circularly polarized light is employed to avoid directionally-dependent polarization effects in the absorption.

In this study, we employed a 42 kg/mol PS-PDMS (31 kg/mol-11 kg/mol) BCP trapped in a metastable state consisting of spherical micelles after spin-coating and utilize the FLaSk anneal to transform to the equilibrium phase (*i.e.* cylindrical PDMS domains). From a zone anneal standpoint, PS-PDMS is strongly segregating (room temperature $\chi N \approx 95$, where χ is the interaction parameter and N is the degree of polymerization) and the ODT (~3000 °C) is not reached before significant polymer degradation. The ODT of PS-

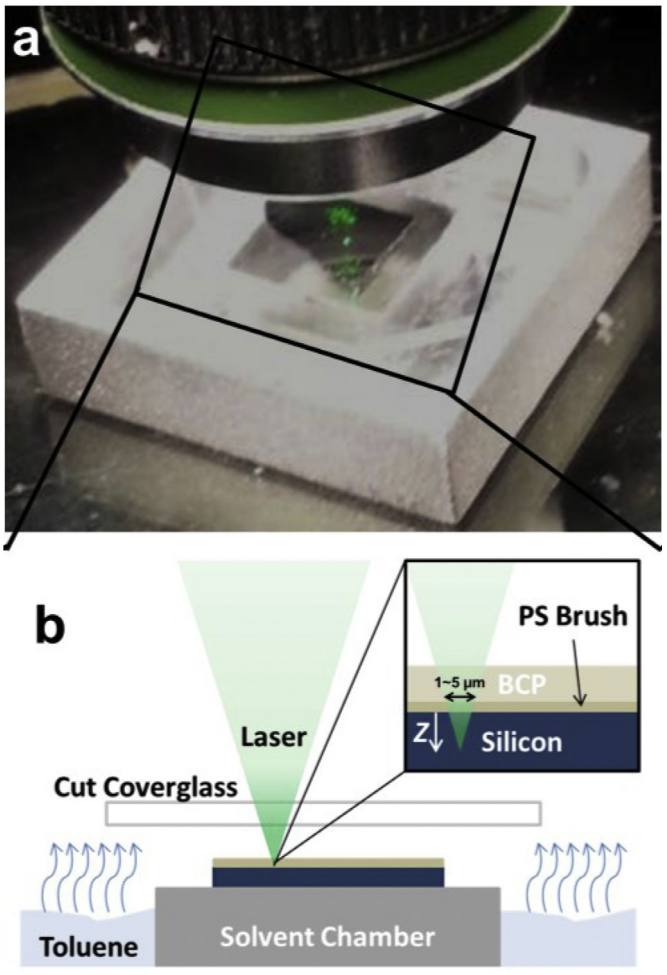

Fig. 1. Photograph (a) and schematic (b) of FLaSk zone annealing solvent setup. The solvent chamber (grey aluminum box in (a)) includes a platform surrounded by a solvent reservoir. The sample is placed on the platform underneath a cut cover glass. The surrounding solvent reservoir is filled with solvent (here, toluene) which slowly evaporates to generate a steady-state partial pressure of solvent under the cover glass. For the patterning, the BCP is spun on top of a PS brush on a silicon wafer, and the circularly polarized laser is focused through the glass with spot size controlled by axial translation away from surface "in-focus" position (Z).

PDMS was only recently observed for the first time by our group in ultrahigh energy impact [33], where adiabatic compression of Mach 1.5 projectiles resulted in massive, nearly-instantaneous adiabatic heating. For these reasons, the temperatures generated by FLaSk (definitely <1400 °C due to silicon damage threshold) allow it to be classified as a cold zone annealing for this particular BCP with thermal gradients orders of magnitude greater than those previously explored. Further, the incorporation of solvent adds the benefits of high-temperature solvent annealing, which was recently demonstrated as a means to enhance the kinetics of BCP ordering in the PS-PDMS BCP system [12].

2. Experimental

2.1. Thin film preparation

Lightly doped p-type silicon substrates ([100] orientation, 10 Ω cm) were coated with hydroxyl terminated polystyrene (M_n = 3000 kg/mol, PDI = 1.06, PolymerSource P2969-SOH) and heated to 170 °C for 16 h in a vacuum oven, which induced binding of the hydroxyl groups to the native oxide. Then the wafers were rinsed with toluene to remove the unreacted brush layers after which BCP films of PS-PDMS (31 kg/mol-11 kg/mol, PolymerSource) were spun from 1.8 wt% solutions in PGMEA to prepare films of 49–55 nm thickness. The film thickness was determined by ellipsometry, corrected for total thickness of oxide and brush (~8 nm), with a J. A. Woollam Co. M-2000D spectroscopic ellipsometer. Swelling ratio was determined with a Filmetrics, Inc., F20 UV, 250–1500 nm spectroscopic reflectometer by comparing the dry films and films inside of the solvent chamber used for the laser writing experiments. By using the same chamber, results were expected to be consistent between the interferometer and the laser stage. Film thickness in these conditions was stable for 30–40 min allowing sufficient time for patterning before gradually deswelling as the solvent supplied from the reservoir was depleted. Samples were removed from the solvent chamber immediately after patterning.

2.2. FLaSk zone annealing

FLaSk zone annealing was performed using circularly polarized 532 nm light from a Coherent Verdi V5 diode pumped solid state laser system. Power was controlled by the system controller and measured with a power meter (Newport 818-UV) using an in-path partially reflecting mirror placed before the lens. The power meter was also positioned after the objective to determine the amount of light that reached the sample relative to the standard positioning of the meter. The objective lens used was a Zeiss LD Achroplan 20× objective with numerical aperture 0.4. The last optic before the objective was a green dielectric mirror, allowing for simultaneous imaging in transmission with red and near-IR light from a white light source *via* a camera mounted above the stage. Motion of the sample for direct write was controlled by a Physik Instruments PIMars™ piezostage with 300 μm of travel on all three axes mounted on a PI M-686 stage for larger motion. Patterning was controlled by a LabView program that controlled both the stage and an electronic shutter. To incorporate solvent swelling, samples were surrounded with a trough of toluene, with the vapor pressure controlled by a cut glass cover as shown in Fig. 1. As the toluene evaporates, a partial pressure of toluene is established over the sample. The size of the cut cover glass was as large as would not result in condensation, which provided maximum uniformity to the achieved pressure, corresponding to swelling of ~140% as measured by reflectometry detailed above. Writes were performed as close to the center of the sample holder as possible in order to assist with stability. For consistency, both samples with and without solvent were patterned through the same glass, compensated by a correction setting on the objective for 1 mm of glass. Detailed chamber measurements are in the Supplementary Information.

2.3. Imaging

After FLaSk annealing, PS-PDMS was exposed to a 5 s, 10 m Torr tetrafluoromethane reactive ion etch at 90 W followed by a 22 s, 10 m Torr oxygen reactive ion etch in order to etch the PS matrix and reveal the underlying oxidized PDMS morphology. After coating with 12–16 nm of AuPd with a Quorum Technologies Polaron SC7640, scanning electron microscope (SEM) imaging was performed on a JEOL 6700 microscope at 5 keV with 6 mm working distance. atomic force microscope (AFM) imaging in Supplementary Information was performed with a Veeco Dimension 3100.

2.4. Simulations

Simulations of the FLaSk process were conducted through FEM simulations using the commercial package, COMSOL Multiphysics. For this study, we used the package for thermal conduction.

3. Results and discussion

As with our earlier work [32], finite element method (FEM) simulations were utilized to estimate the temperatures and temperature gradients that the polymer would experience during the FLaSk anneal. The thermal profile was analytically modeled as arising from a Gaussian light source (NA = 0.4) causing local optical absorption and heating. Temperature-dependent materials properties were utilized for the thermal conductivity, heat capacity, and density of the silicon substrate [34]. The optical absorption also displays an exponential dependence on temperature, so it was simulated using a previously derived empirical model for near-intrinsic silicon excited with 532 nm light [35]. Finally, the absorbed power by the substrate was calibrated by measuring the damage threshold, which corresponds to a peak temperature of ~1400 °C at which the silicon surface melts [36]. Utilizing a steady state approximation with these empirical parameters, the simulated peak temperatures and gradients as a function of measured laser beam power (before objective and cover glass reflection) focused on the surface are shown in Fig. 2a for three scenarios. These represent the temperatures determined for a bare wafer (black trace, 17.5% optical energy absorption), a calculated value for the bare wafer with a 50 nm polymer antireflection coating of average index (1.55) corresponding to the BCP (dark grey, possessing a lower reflectivity and higher absorption of 20.8%), and the calculated curve using the observed damage threshold during the actual annealing experiments (light grey, 18.9% absorption). Due to the fact that the patterned lines are observed to thin through the thermocapillary effect, even at constant power, the temperature progresses from the dark grey trace to the black as the film thins, resulting in a temperature near the light grey trace. Under the hypothesis of the thermal gradient being the key factor, it is significant that for the laser powers utilized (300–350 mW, corresponding to an average temperature of approximately 200–300 °C), gradients on the order of 100–750 K/μm are created. The temporal gradient can be approximately determined by the spatial gradient multiplied by the write speed, corresponding to temporal thermal gradients on the order of 3000–75,000 K/s depending on write speed (30–100 μm/s). These are two to four *orders of magnitude* greater than those used in the previous cold zone annealing studies [25–30]. The spatial temperature and gradient profiles are shown in Fig. 2b for a peak BCP film temperature of

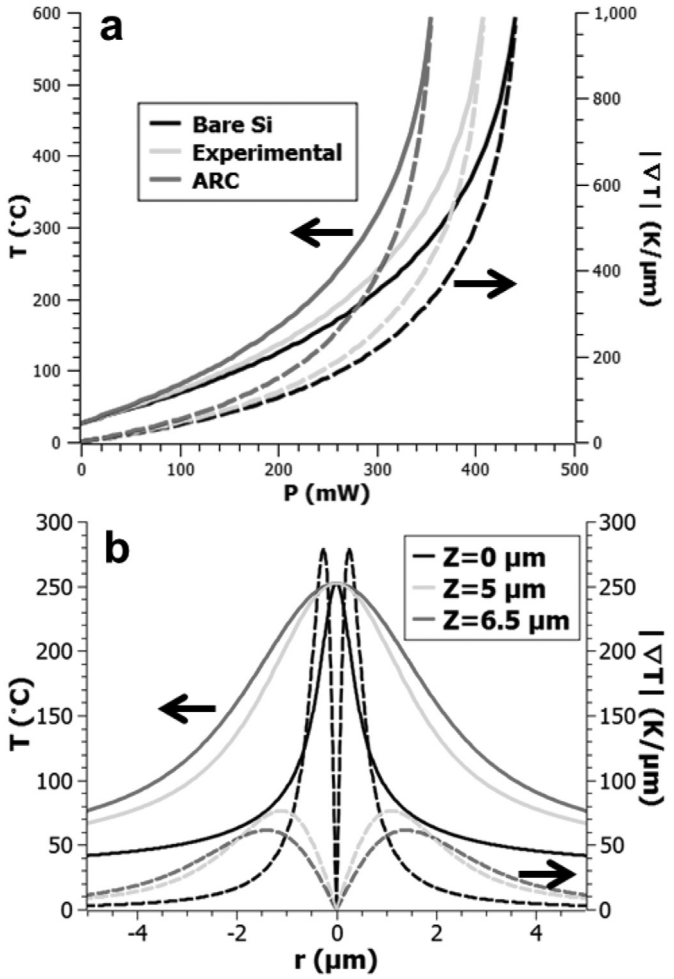

Fig. 2. (a) FEM simulation of the peak temperature and spatial thermal gradient experienced by a central point along a FLaSk write path focused in the plane of the substrate surface for bare silicon (black), experimental BCP (light grey), and the high limit of the full BCP film acting as an antireflection coating (dark grey). (b) Temperature (solid) and gradient-magnitude (dashed) profiles for three differing focus laser spots (the zero-defocus profile is from Ref. [32]) from the surface of the sample. Here, the BCP thickness is considered negligible for the purpose of defining focus, which is also considered as independent of the silicon refractive index (*i.e.* free space focal translation). (For interpretation of the references to color in this figure legend, the reader is referred to the web version of this article.)

250 °C, demonstrating the tunability by changing the focus ($Z = 0$ [32], 5, and 6.5 μm offsets) to control the effective spot size from 0.5 to 3 μm, here defined as the distance between peak gradients.

To create an initial metastable state, the PS-PDMS BCP was spun from a propylene glycol monomethyl ether acetate (PGMEA) solvent that was preferential for PS leading to a film consisting of spherical micelles with the minority PDMS blocks at the core, as previously described for this BCP composition [13], with PS-air and PS-PS-brush contact surfaces. The purpose of the brush being to reduce the tendency for the BCP to dewet completely. The micelles pack into a monolayer hexagonal array, as opposed to the equilibrium cylindrical phase, without a PDMS surface layer which typically forms in annealed PS-PDMS films due to the lower surface energy of PDMS. Subsequent morphological changes during FLaSk annealing are therefore not affected by any directional bias from preexisting cylindrical microdomains. While a fully disordered film may provide a better initial state for the annealing experiments, spin coating of the PS-PDMS from any solvent led to micelles or microphase separation in the as-cast film.

Films were swollen to 140% of their as-cast thickness using toluene vapor during the writing process (as measured by reflectometry) which was attributed to a vapor pressure of toluene of approximately 19 Torr (~85% of the saturation vapor pressure, as determined by previously reported reflectometry measurements) [37]. While this increased the mobility of the film, it was insufficient to allow changes in the morphology of spherical micelles in the absence of FLaSk heating during the time scale of a given experiment (~30 min). Further, toluene, even at complete saturation does not initiate the ODT of the BCP up to the boiling point, as shown in the solvothermal annealing study [12]. At these molecular weights, the individual chains are likely not highly entangled (M_e = ~13 kg/mol and ~12 kg/mol for PS and PDMS respectively) [38]. We expect that the major contribution of the solvent, beyond increasing mobility of the PS chains, was to induce evaporative cooling during the onset of annealing leading to a sharper thermal gradient. Isolation of these two effects is complicated by the inability to swell the film without changing the mobility, but the presence of a significant thermal effect was supported by observations of the electron contrast in the surrounding heated region. Fig. 3 shows a series of single-pass lines written at different focuses with respect to the plane of the substrate for films with and without solvent vapor. Without solvent, the bright region in the post-etch SEM images surrounding a given patterned line (attributed by pre-etch AFM results as arising from rough, dewetting-induced ridges surrounding the patterned lines (Fig. S1)) is ~5× the apparent annealed width, while little or no similar effect is observed in the presence of solvent, indicating a reduction in the extent of the thermal effect. As the samples are swollen with solvent rather than immersed, it can be expected that the solvent will be almost completely removed at the highest-temperature portion of the spike, thus allowing for the peak annealing temperature to be reached and resulting in a sharpened gradient while simultaneously reducing the solvent-induced mobility effects. Due to the complexity of the combined solvent and thermal anneal with rapid removal of solvent, we leave more predictive simulations for future work.

Images of selected lines patterned by the 532 nm laser are shown along with the 2D Fourier transforms of the laser annealed

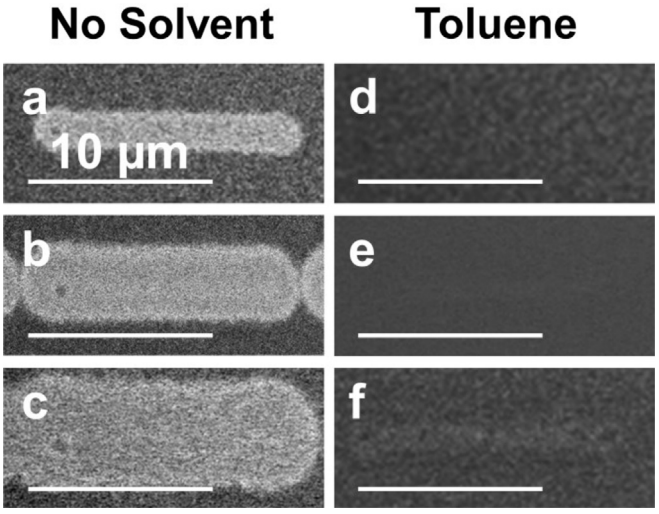

Fig. 3. Low-magnification SEM images of characteristic single-pass FLaSk lines patterned with focus at 0 μm (a,d), 5 μm (b,e), and 6.5 μm (c,f) below the surface of the substrate without (a, b, c) and with (d, e, f) toluene vapor. The width of the bright region is present to a much larger extent in the lines patterned without solvent indicating a larger area of heated polymer due to the lack of evaporative cooling.

region in Fig. 4a–d. Despite the very short anneal times, formation of cylindrical microdomains occurred in which the cylinders were preferentially aligned along the writing direction, as can be further seen by the asymmetry in the Fourier transforms. Domain size in the annealed region appears larger than the surrounding unannealed region due to relaxation of the kinetically-trapped, collapsed PDMS micelles (~35 nm center-to-center spacing) to the equilibrium domain spacing (39–42 nm period as compared to 38 nm, Fig. S2). Line widths, which could be controlled by adjusting the laser focus, exhibited sub-wavelength resolution due to the strong nonlinearity of this process – the in-focus patterned regions have typical line widths between 0.3 and 0.5 μm, compared to the expected spot size of 0.85 μm. The FLaSk-induced transformation only occurs for a specific processing window, illustrated in Fig. 5a for samples with and without solvent vapor. Only patterns where a majority of the expressed morphology was cylinders are plotted, excluding mixed-morphology lines.

When the dose was too low, the spheres relaxed, but did not fully transform, as would be expected from the heat-quench mechanism (shown as top inset of Fig. 5a for $Z = 6.5$ μm); however, when the dose was too high (high power and/or low speed), two distinct behaviors were observed. The first was a complete dewetting of BCP in the annealed region. This is an expected result as all of the lines were seen visually to thin during the annealing due to thermocapillary dewetting effect [32], necessitating the use of thicker films (49–55 nm) than required for a monolayer of BCP microdomains (~30 nm [13]). The second was the observation of spheres possessing the same dimension as the collapsed micelles in the as-cast film surrounded by cylinders, which indicates that the temperature was high enough that the PDMS fully degraded or crosslinked during the anneal (shown as bottom inset of Fig. 5a for $Z = 0$ μm). The effect of the solvent was to broaden the processing window, especially for deeper defocuses (5 and 6.5 μm), by sharpening the effective gradient.

Cylinder alignment for the solvent annealed samples as determined by the localization of the first order Fourier transform peak of the annealed region was also analyzed with extracted full-width at half-maximum (FWHM) of the angular peak shown in Fig. 5b. From these lines, the in-plane orientation of cylinders within a range of angular FWHM of 80-110° can be observed, with the minimum FWHM sample corresponding to the image shown in Fig. 4b. The general trend is increasing alignment with speed for a given writing power, and wider lines (created by focus beneath the BCP layer) possessing overall better alignment. The latter observation is to be expected as a narrower line width (given a similar magnitude of the gradient) experiences greater confinement from the surrounding immobile polymer and, perhaps more importantly, side gradient effects (discussed below) have a greater influence on the distribution of alignments. Though the scan speed is limited here to 100 μm/s due to the stage accuracy, ongoing experimentation has demonstrated ordering for speeds up to 1000 μm/s, so the limitations of the ordering rate (set by mass transport) have not yet been reached.

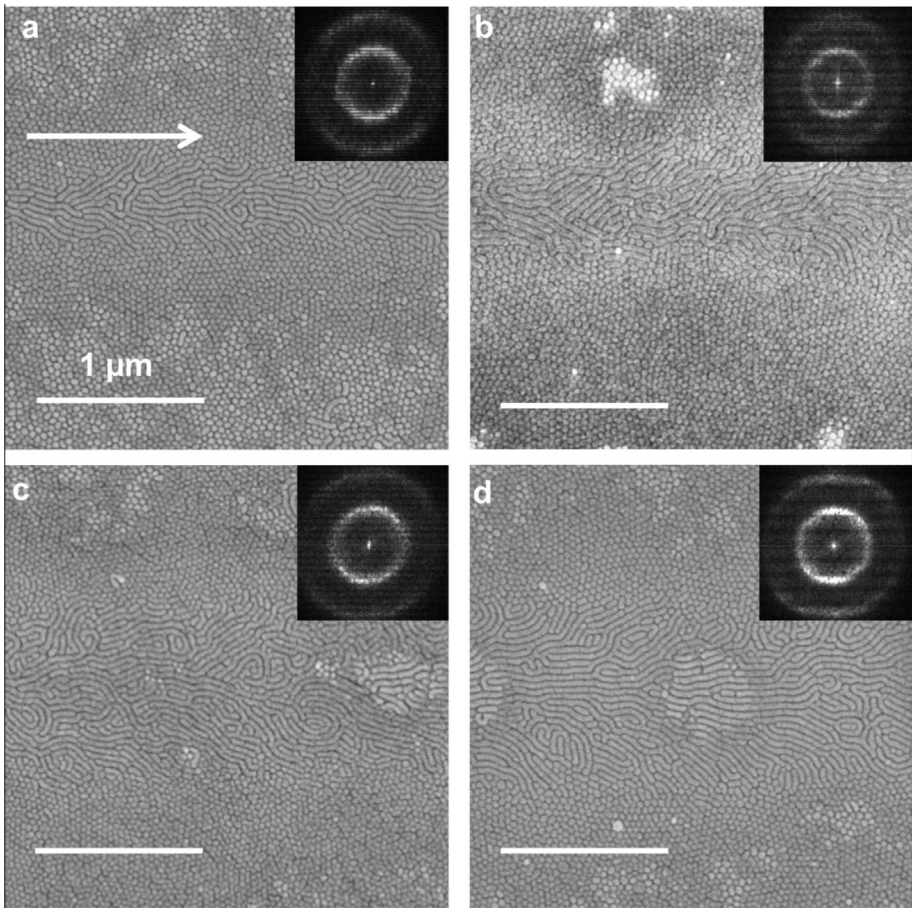

Fig. 4. (a–d) SEM images of some characteristic FLaSk patterned lines. Horizontal lines are written within solvent-swollen BCP films left-to-right for different speeds and powers at three focuses: (a) 335 mW, 60 μm/s for focus at the substrate surface; (b) 500 mW, 30 μm/s for focus 5 μm below the surface; (c) 625 mW, 30 μm/s and (d) 635 mW, 100 μm/s for focus 6.5 μm below the surface. 2D Fourier transforms of the cylindrical morphology regions (inset) confirm the preferential alignment.

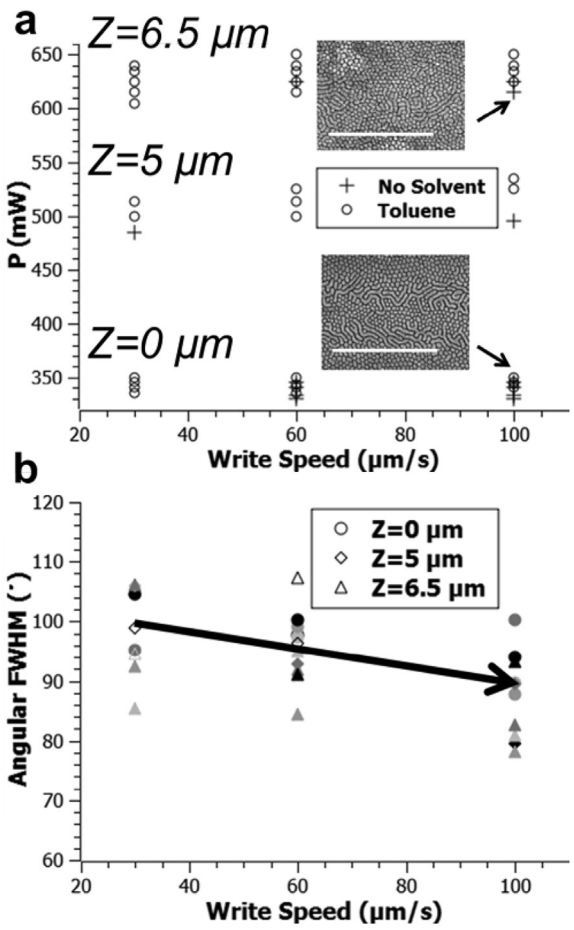

Fig. 5. (a) Conditions that resulted in formation of a line with predominantly cylindrical morphology. Each symbol corresponds to a sample. For comparison, the samples processed without (crosses) and with (empty circles) solvent are also included. Examples of samples outside of the processing window are shown as insets with the lower inset characteristic of too high of a dose at $Z = 0$ μm and the upper inset characteristic of too low of a dose at $Z = 6.5$ μm. Inset scale bars are 1 μm. (b) Assessment of the degree of alignment for samples patterned in toluene solvent vapor, as defined by the angular deviation of the anisotropic 2D Fourier transform of the annealed regions for solvent annealed FLaSk samples. Samples are grouped by focus, with darker samples corresponding to higher power writes within the processing window identified in (a). Linear fit of the data is shown as an arrow indicating the general trend of enhanced alignment with increasing speed.

Beyond the patterning capability, the results obtained by FLaSk zone anneal offer insight into the mechanisms of cold zone annealing. First, it is important to differentiate the ordering mechanism from other phenomena occurring during the anneal, such as dewetting. It is tempting to link these two behaviors, especially as the flow-field generated by dewetting would be in the observed direction of alignment and could be analogous to similar elongational flow alignment obtained in electrospun BCP fibers [39]. Counter to this explanation is the lack of any observation of film thinning in previous cold zone annealing studies of BCPs, though thermocapillary dewetting of higher mobility surfactant-phenolic resin ordered assemblies in *static* thermal gradients was used as a part of a recent cold zone study to qualify the importance of relative mobility and crosslinking in the gradient for zone annealing of a thermocrosslinking system [27]. This supports the conclusion that mass transport is limited during the *moving* cold zone annealing and is, therefore, not the critical factor. Further against the conclusion of mass transport being the key mechanism is the fact that dewetting often occurred *without* simultaneous alignment, such as in lines written at low (<30 μm/s) speed. Indeed, the only samples where significant regions of alignment purely perpendicular to the writing direction were observed were the highest focus lowest speed (3 μm/s) lines conducted at powers corresponding to typical thermal anneals (~225 °C, Fig. 6). These samples predominantly show horizontal alignment perpendicular to the write direction, as opposed to the parallel alignment dominant in the majority of lines. The faster lines do exhibit features suggestive of perpendicular alignment near the edges of the lines, where the cylinders cant outward, but always with a bias towards the direction of the writing. This canting is likely the greatest impediment to obtaining good cylinder orientation by FLaSk zone annealing as it competes with the alignment along the write direction. The canting may be correctable by, for example, using a focal spot with an elliptical point spread function. The purposefully asymmetric thermal gradients would be expected to increase the alignment bias along the short axis. Also it remains to see how templated structures behave where FLaSk is aided by additional influences on preferred domain directions.

These two observations support the magnitudes and sequence of the thermal gradients being the key factors in determining the alignment and also differentiate the perpendicular alignment from that predicted in existing models of moving mobility gradients [40,41]. Rather, in the case of the slow speed lines, the perpendicular alignment is initiated by the side gradients occurring just after the onset of parallel alignment, breaking up the order of the central cylinders. The second parallel gradient (*i.e.* cooling) did not initiate additional reordering, consistent with the experimental cold zone observations. The generation of partial perpendicular alignment in slow lines has only been demonstrated with a low relative order for the tightest focus, and parallel alignment in these slow lines was not observed. This suggests that there is a threshold gradient that needs to be achieved in order to induce ordering and alignment. The presence of parallel alignment in fast lines and low order in perpendicular alignment in slow lines further indicates that the threshold is related to the *temporal* gradient, which increasingly favors the writing direction as the speed increases. This explanation is supported by the trend in ordering discussed above.

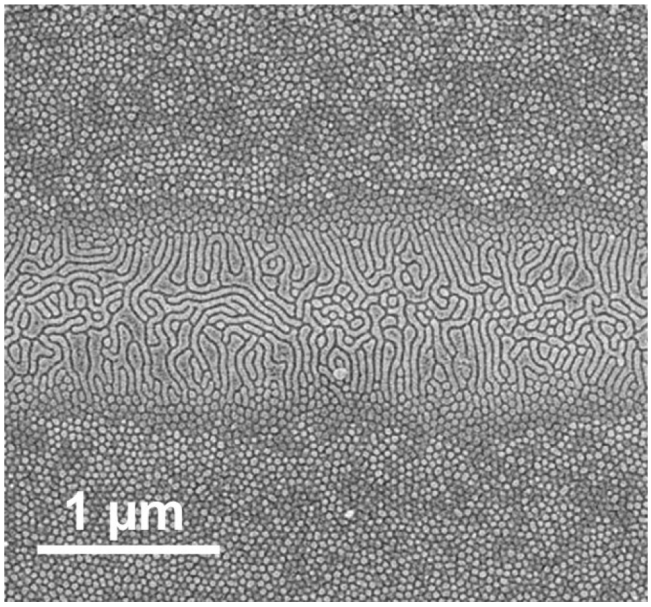

Fig. 6. FLaSk line patterned at low power (285 mW) and low speed (3 μm/s) of a surface-focused beam resulting in cylinder alignment perpendicular to the writing direction.

What remains to be understood is the driving force for the gradient-mediated alignment. As mentioned earlier, it does not appear to be caused by mass transport, though this is presumably the limiting factor both at low speeds due to the dewetting and high speeds due to a kinetic limitation. One possible cause is film shears that also serve as the driving force for dewetting. Shear has been shown as an effective way to align BCP microdomains [42,43], including in recent cold zone studies [28]. Thermocapillary shear is generally expressed as $\tilde{\tau}\cdot\hat{n} = \nabla\gamma = (d\gamma/dT)\nabla T$ [44,45], where $\tilde{\tau}$ is the shear stress, $\hat{n}$ the surface normal, and γ the surface tension. The surface tension almost always decreases with temperature leading to a net force down the thermal gradient. By approximating the surface as pure molten polystyrene ($d\gamma/dT = -0.07$ mN/m·K) [46] stresses on the order of 10–100 kPa for the gradients utilized in this experiment are calculated. This is consistent with the high end of values for external shear stresses used in alignment studies.

It should be noted that the reframing of surface tension gradient in terms of the thermal gradient is not strictly applicable in the case of solvent-swollen FLaSk experiments, where the thermal removal of solvent from the film also affects the spatial profile of the surface energy. This is a relatively unique mechanism to FLaSk annealing, since most solvent swelling gradients, such as the ones provided by rastered nozzle writing [15], are relatively diffuse. In contrast, with FLaSk, the film can be expected to transition from swollen to dry over a similar length scale as the thermal gradient (*i.e.* sub-micron). If we consider as a first approximation that, for PS, $\Delta\gamma$ at a peak temperature of 300 °C is on the order of $-\gamma$ ($\gamma = 31.0$ mN/m) [46], then for the gradient of the solvent concentration to have a similar magnitude effect, it would have to alter the surface tension by a similar factor. Prior simulations have indicated that solvent vapor effects on surface tension can be expected to be of this magnitude and therefore, a "solvocapillary" shear force due to solvent gradient may be expected to be one additional contribution. The removal of solvent, however, can be expected to *increase* the surface tension, suggesting that the solvocapillary shear would be in the opposite direction of the thermocapillary shear. This view is over-simplistic, however, as the value of $d\gamma/dT$ can also be expected to be affected by the solvent (though to the authors' knowledge this has not been studied), coupling these two effects. Were the incorporation of solvent to increase the negative magnitude of $d\gamma/dT$ (an intuitive result) the "conventional" thermocapillary stress would be enhanced, consistent with the observation of alignment only during the heating portion of the gradient, as the line immediately behind the moving laser spot would be expected to still be dry.

There are also complex effects due to thermal expansion-induced strains within the polymer film itself. This is likely enhanced both due to constrained expansion along the gradient and mismatches between the constituent blocks. Thermal expansion gradients were proposed as a mechanism for the observed vertical alignment in samples submitted to relatively "sharp" conventional cold zone thermal gradients [29]. As vertical alignment was not observed in this experiment, despite the much sharper nature of the spatial and temporal gradient, it can be expected that these results represent a regime where the contributions of the thermocapillary driving force overcomes the driving forces for vertical alignment, possibly also reduced by the simultaneous contraction that occurs as the solvent is removed from the film.

The ability of this technique for making more complex patterns was demonstrated by annealing in a circular write path at a focus of $Z = 5$ μm to determine if the orientation control could match a constant alteration in the writing direction. A SEM image of the highest curvature available (0.20 μm^{-1}, corresponding to ~2 revolutions per second; additional examples in Fig. S3) with domain orientation mapping is shown in Fig. 7 indicating that it is still possible to obtain orientational tracking of the moving beam even with path curvature, though the limits of this alignment need to be tested beyond the capabilities of our patterning system. The orientational map shows the orientation error (*i.e.* the deviation from perfect circular tracking). On the inside of the path, the map is bluer, representing an enhanced domain tilt inward, while the outside of the path shows an outward domain tilt. This is consistent with the effects of the outward canting of the cylinders due to the moving side gradients discussed above.

4. Conclusion

By an application of a FLaSk zone annealing we have demonstrated a method for driving transformation of a metastable thin film of a strongly segregating BCP toward its equilibrium microdomain morphology as well as controlling the orientation of the domains. This is accomplished with a sub-second thermal anneal possessing thermal gradients on the order of 100–750 K/μm (3000–75,000 K/s), which additionally leads to alignment of the generated cylinders along the writing direction analogous to larger scale cold zone annealing experiments, with a likely mechanism

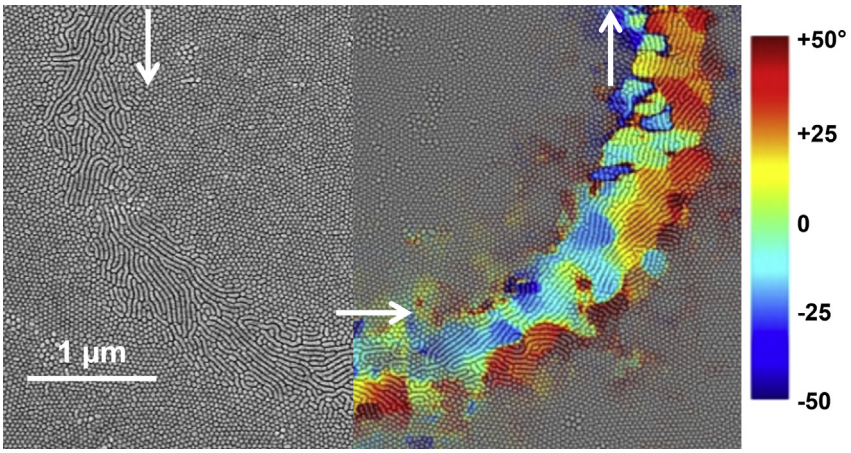

Fig. 7. Portion of a 5 μm diameter circular counter clockwise path written with a 545 mW beam moving at 60 μm/s focused 5 μm into the silicon. Domain alignment can be observed to track the writing direction. This is further confirmed by alignment mapping (right side color map), with much of the observed deviation correlating with the outward canting of boundary domains (dark red and blue regions) as can be seen when the alignment is compared to perfect circumferential orientation (green regions).

being thermocapillary shear. Based on the observations of both the lines patterned at high and low speeds, it appears that the temporal thermal gradient is the key driving force for the preferential alignment, with faster write speeds leading to a higher degree of orientational order, with the angular FWHM of the cylindrical microdomain axes as narrow as 80°. This annealing was performed at a previously unprecedented speed, occurring in 10–100 ms. Including solvent vapor in the sample chamber resulted in film swelling and subsequent evaporative cooling. To the best of our knowledge, this is the first application of incorporating solvent vapor in a sub-micron direct write or zone annealing process. In this case, the effect of solvent was to increase mobility and increase the thermal and surface energy gradients, leading to an expanded processing window. Even with solvent, the processing window was only ~5% absolute power, corresponding to only tens of °C temperature differences. Despite this, the technique still represents a highly scalable method of controlling the in-plane alignment of BCP self-assembly and producing films that incorporate multiple morphologies by converting large-area cold zone annealing into sub-micron direct write. Based on ~1 μm wide lines patterned at ~1 mm/s, raster-based patterning could occur at ~1000 $\mu m^2/s$, though proximity effects of adjacent lines will have to be considered. While currently there are limitations to the quality of ordering as compared to other methods, the parameter space of both FLaSk and conventional cold zone annealing has just begun to be explored, including the effects of using different BCP molecular weights, compositions, and volume fractions. Further, the use of solvent vapors with different block preference and boiling points represents a previously unconsidered (for zone annealing) parameter that can potentially lock greater ordering and alignment enhancement and even further degrees of freedom in morphology manipulation, and the use of different beam profiles can both reduce the effects of side gradients and also enhance the overall patterning rate. Overall, FLaSk zone annealing has the potential to provide a compromise between the precision of microdomain ordering achievable by e-beam patterning and the high throughput achievable by zone or shear alignment, or in combination with templates produced by, for example, imprint or interference lithography, FLaSk zone annealing could offer a method to introduce local orientation control.

Acknowledgment

This research was supported (in part) by the U.S. Army Research Office under contract W911NF-07-D-0004, by the Semiconductor Research Corporation, TEL and TSMC. J. Singer was supported by the Department of Defense (DoD) through the National Defense Science & Engineering Graduate Fellowship (NDSEG) Program. The authors would like to acknowledge M. Tarkanian for his assistance in machining the solvent reactor and A. Hannon, A. Alexander-Katz and T. Epps III for valuable discussions.

Appendix A. Supplementary data

Supplementary data related to this article can be found at http://dx.doi.org/10.1016/j.polymer.2014.02.028.

References

[1] Bates FS, Fredrickson GH. Annu Rev Phys Chem 1990;41(1):525–57.
[2] Stoykovich MP, Kang H, Daoulas K, Liu G, Liu CC, de Pablo JJ, et al. ACS Nano 2007;1(3):168–75.
[3] Edwards EW, Montague MF, Solak HH, Hawker CJ, Nealey PF. Adv Mater 2004;16(15):1315–9.
[4] Son JG, Chang J-B, Berggren KK, Ross CA. Nano Lett 2011;11(11):5079–84.
[5] Ross CA, Jung YS, Chuang VP, Son JG, Gotrik KW, Mickiewicz RA, et al. Proc SPIE 2010;7637:76370H–7H.
[6] Jung YS, Jung W, Ross CA. Nano Lett 2008;8(9):2975–81.
[7] Ruiz R, Ruiz N, Zhang Y, Sandstrom RL, Black CT. Adv Mater 2007;19(16):2157–62.
[8] Cheng JY, Ross CA, Thomas EL, Smith HI, Vancso GJ. Appl Phys Lett 2002;81(19):3657–9.
[9] Bita I, Yang JKW, Jung YS, Ross CA, Thomas EL, Berggren KK. Science 2008;321(5891):939–43.
[10] Mori K, Hasegawa H, Hashimoto T. Polymer 1990;31(12):2368–76.
[11] Lo T-Y, Chao C-C, Ho R-M, Georgopanos P, Avgeropoulos A, Thomas EL. Macromolecules 2013;46(18):7513–24.
[12] Gotrik KW, Ross CA. Nano Lett 2013;13(11):5117–22.
[13] Hsieh IF, Sun H-J, Fu Q, Lotz B, Cavicchi KA, Cheng SZD. Soft Matter 2012;8(30):7937–44.
[14] Bosworth JK, Black CT, Ober CK. ACS Nano 2009;3(7):1761–6.
[15] Seppala JE, Lewis 3rd RL, Epps 3rd TH. ACS Nano 2012;6(11):9855–62.
[16] Onses MS, Song C, Williamson L, Sutanto E, Ferreira PM, Alleyne AG, et al. Nat Nano 2013;8(9):667–75.
[17] Gat A, Gerzberg L, Gibbons JF, Magee TJ, Peng J, Hong JD. Appl Phys Lett 1978;33(8):775–8.
[18] Chong YF, Gossmann HJL, Pey KL, Thompson MO, Wee ATS, Tung CH. IEEE T Electron Dev 2004;51(5):669–76.
[19] Shima A, Hiraiwa A. Jpn J Appl Phys 2006;45(7):5708.
[20] Jung B, Sha J, Paredes F, Ober CK, Thompson MO, Chandhok M, et al. Proc SPIE 2010;7639:76390L–9L.
[21] Jung B, Chandhok M, Younkin TR, Ober CK, Thompson MO. J Photopolym Sci Technol 2011;24(5):487–90.
[22] Jaw-Luen T, Ming-An T. Rapid formation of block copolymer thin film based on infrared laser irradiation. In: CLEO-PR 2007. Seoul, Korea: Optical Society of America; 2007. ThP_082.
[23] Mita K, Tanaka H, Saijo K, Takenaka M, Hashimoto T. Macromolecules 2007;40(16):5923–33.
[24] Hashimoto T, Bodycomb J, Funaki Y, Kimishima K. Macromolecules 1999;32(3):952–4.
[25] Yager KG, Fredin NJ, Zhang X, Berry BC, Karim A, Jones RL. Soft Matter 2010;6(1):92–9.
[26] Berry BC, Bosse AW, Douglas JF, Jones RL, Karim A. Nano Lett 2007;7(9):2789–94.
[27] Xue J, Singh G, Qiang Z, Karim A, Vogt BD. Nanoscale 2013;5(17):7928–35.
[28] Singh G, Yager KG, Berry B, Kim H-C, Karim A. ACS Nano 2012;6(11):10335–42.
[29] Singh G, Yager KG, Smilgies D-M, Kulkarni MM, Bucknall DG, Karim A. Macromolecules 2012;45(17):7107–17.
[30] Singh G, Batra S, Zhang R, Yuan H, Yager KG, Cakmak M, et al. ACS Nano 2013;7(6):5291–9.
[31] Singer JP, Kooi SE, Thomas EL. Nanoscale 2011;3(7):2730–8.
[32] Singer JP, Lin P-T, Kooi SE, Kimerling LC, Michel J, Thomas EL. Adv Mater 2013;25(42):6100–5.
[33] Lee J-H, Veysset D, Singer JP, Retsch M, Saini G, Pezeril T, et al. Nat Commun 2012;3:1164.
[34] Shanks HR, Maycock PD, Sidles PH, Danielson GC. Phys Rev 1963;130(5):1743–8.
[35] Jellison JGE, Modine FA. Appl Phys Lett 1982;41(2):180–2.
[36] Lo HW, Compaan A. J Appl Phys 1980;51(3):1565–8.
[37] Gotrik KW, Hannon AF, Son JG, Keller B, Alexander-Katz A, Ross CA. ACS Nano 2012;6(9):8052–9.
[38] Fetters LJ, Lohse DJ, Richter D, Witten TA, Zirkel A. Macromolecules 1994;27(17):4639–47.
[39] Ma M, Titievsky K, Thomas EL, Rutledge GC. Nano Lett 2009;9(4):1678–83.
[40] Zhang H, Zhang J, Yang Y, Zhou X. J Chem Phys 1997;106(2):784–92.
[41] Bosse AW, Douglas JF, Berry BC, Jones RL, Karim A. Phys Rev Lett 2007;99(21):216101.
[42] Pujari S, Keaton MA, Chaikin PM, Register RA. Soft Matter 2012;8(19):5358–63.
[43] Angelescu DE, Waller JH, Adamson DH, Deshpande P, Chou SY, Register RA, et al. Adv Mater 2004;16(19):1736–40.
[44] Brochard F. Langmuir 1989;5(2):432–8.
[45] Ludviksson V, Lightfoot EN. AlChE J 1971;17(5):1166–73.
[46] Pu Z. In: Mark JE, editor. Polymer data handbook. NY: Oxford Univ. Press; 2009.